

Solar low-degree p-mode parameters from the GONG network

M.C. Rabello-Soares¹ and T. Appourchaux²

¹ Teoretisk Astrofysik Center, Danmarks Grundforskningsfond and Institut for Fysik og Astronomi, Aarhus Universitet, DK-8000 Aarhus C, Denmark (csoares@obs.aau.dk)

² Space Science Department of ESA, ESTEC, 2200 AG Noordwijk, The Netherlands (thierry@so.estec.esa.nl)

Received 10 November 1998 / Accepted 18 February 1999

Abstract. Low-degree solar p modes observed by the GONG network have been analysed for $l \leq 6$, yielding accurate measurements of their frequencies, splittings and linewidths. The results obtained here show significant improvement on previous determinations, especially for increasing the number of identified modes with $l \leq 3$ and for minimizing the bias on the splitting determination and the error bars. A more realistic approach was used to fit the helioseismic data assuming that the observed spectra are statistically dependent upon one another. This is in contrast to what is commonly done and the result is a better treatment of the leakage between the modes. Moreover, the effect of an imperfect knowledge of the leakage within the elements of the $l = 1$ multiplets upon their splitting determination is analysed. In addition, the effect of the leakage between the modes of different degrees upon the p-mode parameters determination is shown, and a procedure for ‘cleaning’ the spatial alias is described leading to splitting coefficients with smaller systematic errors than before.

Key words: Sun: oscillations – methods: data analysis – methods: observational

1. Introduction

Helioseismology uses the temporal and spatial properties of solar oscillations to study the solar interior. Acoustic modes with a large horizontal wavelength (corresponding to a low spherical harmonic degree l) penetrates deeper into the solar interior than modes with a smaller wavelength. These low-degree modes give us information on the solar core. However, even if our aim is to study only the solar core, the low-degree modes must be combined with high-degree modes because the dominant contributions to the mode eigenfunction come from the outer parts of the Sun. To detect modes with $l > 3$, it is necessary to have observations with spatial resolution.

When the solar image is resolved a very large number of modes can be detected making the data analysis very complicated. In order to extract a single (l, m) mode from resolved observations, spherical harmonic decomposition of each image must be performed. Unfortunately, it is essentially impossible

to isolate individual modes based on their angular dependence alone, because only half of the solar surface is observed.

Since the modes are not completely isolated, the Fourier transform for a given (l, m) mode ($y_{l,m}$) is not given by the Fourier transform of a single mode ($x_{l,m}$), but rather as a sum over several modes, which can be expressed as:

$$y_{l,m}(\nu) = \sum_{l',m'} C_{m,m'}^{(l,l')} x_{l',m'}(\nu) \quad (1)$$

where the sum comprises the modes contributing to the given spectrum and $C_{m,m'}^{(l,l')}$ is the contribution from each mode. C is called the leakage matrix: it is a square matrix with each dimension equal to $\sum_{l'} (2l' + 1)$, where again the sum comprises the modes contributing to the given spectrum (l, m) . The C elements are given by $C_{m,m'}^{(l,l')}$ where a given (l', m') characterizes a column and a given (l, m) a line. C is independent of frequency ν and it is the same for both real and imaginary parts of the Fourier transform (Schou 1992; Appourchaux et al. 1998a, hereafter Paper I). The Fourier spectra of the p modes are normally distributed with a zero mean and variance $v_{l,m}$, which is in general represented by a Lorentzian shape with a set of parameters \mathbf{a} . For obvious reasons, the leakage matrix is normalized as $C_{m,m}^{(l,l)} = 1$. The expected covariance matrix of the real (or the imaginary) part of observed spectra ($y_{l,m}$) is given by:

$$V_{m,m'}^{(l,l')}(\mathbf{a}, \nu) = \sum_{l'',m''} C_{m,m''}^{(l,l'')} C_{m',m''}^{(l',l'')} v_{l'',m''}(\mathbf{a}, \nu) + B_{m,m'}^{(l,l')}(\nu) \quad (2)$$

where $v_{l'',m''}$ is the variance of the real (or imaginary) part of the Fourier spectrum of a single mode ($x_{l'',m''}$) and B is the noise covariance matrix (Paper I). The power spectra give an estimate of the diagonal elements of V (Appourchaux et al. 1998b, hereafter Paper II). B and V have the same dimension as C , and their elements are given by $B_{m,m'}^{(l,l')}$ and $V_{m,m'}^{(l,l')}$ respectively.

This is a rather important point to be considered in fitting the data. Not taking into account or considering in an incorrect manner, the spurious modes on a given (l, m) mode spectrum will produce an erroneous determination of the p-mode parameters, as already discussed by Appourchaux et al. (1995) and

Rabello-Soares et al. (1997). This work presents the results of a very careful analysis of the low degree solar p modes observed by the Global Oscillation Network Group (GONG) with a careful treatment of the spatial leakage of the modes.

2. Data analysis

2.1. Maximum likelihood estimation

We used a maximum likelihood method for fitting the peaks in the observed Fourier spectra. We derived the amplitudes, linewidths, frequencies and noise characteristics represented by \mathbf{a} . Instead of fitting the power spectra ($|y_{l,m}|^2$) by minimizing the well-known expression given by Duvall & Harvey (1986), we have, in this work, fitted the Fourier spectra $y_{l,m}(\nu_i)$ using the equation given by Paper I, and adapted from Schou (1992).

The main difference between the two methods lies in the way they treat the spectrum correlation due to the mode leakage. The first method takes into account only the diagonal terms of the covariance matrix \mathbf{V} , assuming that the observed spectra are statistically independent from each other and have a χ^2 probability density function with 2 degrees of freedom. However, from Eq. (1), the observed spectra are a linear combination of the single modes, i.e. they are statistically dependent upon one another and have a multivariate normal probability density function. In this method, the leakage between the modes is taken into account in a more complete way (for a detailed discussion see our previous work: Paper I and II).

We have applied this fitting technique to 360 days of GONG data starting on 23 August 1995 with a 87% duty cycle. The GONG consists of a network of 6 sites with solar velocity imagers ($\sim 250 \times 250$ pixels) located around the Earth to obtain nearly continuous observations of the Sun's five-minute oscillations (for a detailed description, see Harvey et al. 1996). After extracting a single (l, m) mode by spherical harmonic decomposition, an FFT of the whole time series obtained through the merging of all the sites data is computed. No sidebands are visible due to the high continuity in the data. Fig. 1 shows the power spectra of the time series for $l = 1$ and $n = 21$ modes.

A Lorentzian profile was used as a model of the variance of the spectrum of a single mode (n, l, m) , $v_{l,m}''(\mathbf{a}, \nu)$ or, in a different notation, $v_{nlm}(\nu)$:

$$v_{nlm}(\nu) = \frac{A_{nl|m|}(\gamma_{nl}/2)^2}{(\gamma_{nl}/2)^2 + (\nu - \nu_{nlm})^2} \quad (3)$$

where $A_{nl|m|}$ is the power amplitude, γ_{nl} the full linewidth at half maximum and ν_{nlm} is the central frequency. These parameters (\mathbf{a}) plus the background noise ($N_{nl|m|}$) are the ones that we want to find. We used the same linewidth for the entire multiplet (Appourchaux et al. 1995; Rabello-Soares et al. 1997). Also, we used the same amplitude for the $\pm m$ modes; it is expected that the prograde and retrograde modes have the same amplitude and, in fact, we made some tests where they proved to be very similar. The same background noise is fitted for the $\pm m$ modes with $l \leq 3$. However, for higher degree modes, a simplification was made: the background noise was shown to

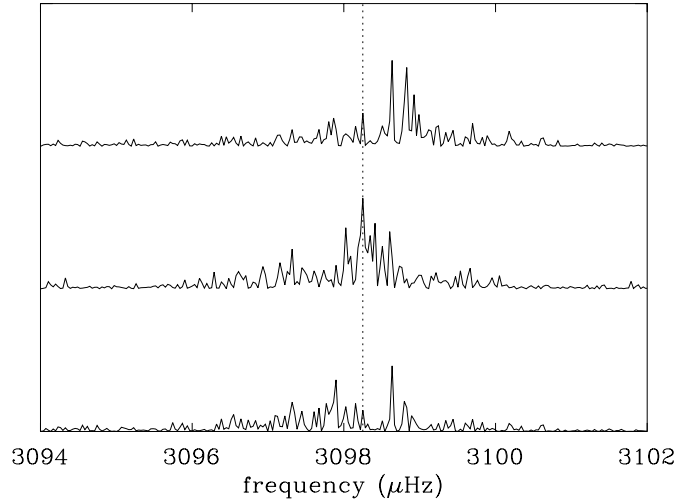


Fig. 1. Power spectra of $l = 1$, $n = 21$ multiplet. From bottom to top, the power spectrum of $m = -1$, 0 and $+1$ modes. The vertical line indicates the mode frequency for $m = 0$. The rotational splitting can be clearly seen as a displacement of $m = +1$ mode towards higher frequency and of $m = -1$ towards lower frequencies. The contribution of $m = +1$ in the $m = -1$ spectrum is seen as a structure of peaks on the right side of the vertical line.

be very similar for all m 's in a multiplet and the convergence of the fitting is easier using only one parameter for the multiplet. We kept the $l + 1$ background noise parameters for low degree modes where the central frequency accuracy is more sensitive to the fitting.

The frequency of the mode (n, l, m) is given by:

$$\nu_{nlm} = \nu_{nl} + \sum_{i=1}^N a_i(n, l) \mathcal{P}_i^{(l)}(m) \quad (4)$$

where ν_{nl} is the mean frequency of the mode multiplet and $\mathcal{P}_i^{(l)}(m)$ are orthogonal polynomials with degree i defined by: $\mathcal{P}_i^{(l)}(l) = l$ and $\sum_{m=-l}^l \mathcal{P}_i^{(l)}(m) \mathcal{P}_j^{(l)}(m) = 0$ for $i \neq j$. The polynomials $\mathcal{P}_i^{(l)}(m)$ can be expressed in terms of the Clebsch-Gordan coefficients (Pijpers 1997). The a_i coefficients measure the frequency splitting due to the solar rotation and are called *splitting coefficients*. We fitted for $l = 1$, a_1 ($N = 1$); for $l = 2$ and 3 , only a_1, a_2 and a_3 ($N = 3$); and for $l \geq 4$, a_1 - a_5 ($N = 5$).

We have fitted around the frequency of a given (n, l, m) mode in a $17\text{-}\mu\text{Hz}$ window for $l \leq 2$, and in a $22\text{-}\mu\text{Hz}$ window for $l \geq 3$. However, when the mode frequency was higher than $4000\text{ }\mu\text{Hz}$, a larger window ($50\text{ }\mu\text{Hz}$) was used to cope with the larger mode linewidth. An estimate of the uncertainties on the fitted parameters was obtained from the inverse of the Hessian matrix (see Paper I).

2.2. Leakage matrix computation

An important point in the p-mode parameter determination is the correct calculation of the leakage matrix \mathbf{C} (Eq. 1) in fitting the power or Fourier spectra. Following Schou & Brown (1994),

the calculation of the leakage matrix C of the GONG data was described in Paper II.

The leakage matrix has some interesting properties. When $l + l' + m + m'$ is odd, its elements are zero because of the parity of the spherical harmonics. The leakage between modes with different m 's but the same l are such that: $C_{-m,0}^{(l,l)} = C_{m,0}^{(l,l)}$, $C_{0,-m}^{(l,l)} = C_{0,m}^{(l,l)}$ and $C_{-m,-m}^{(l,l)} = C_{m,-m}^{(l,l)}$, resulting in l^2 elements to be calculated in a given multiplet. Note that, in this case, C is not symmetrical after applying the normalization $C_{m,m}^{(l,l)} = 1$. In the following sections, only the leakage within a given multiplet will be considered. Only in Sect. 3.3 will the problem of leakage between different l 's be addressed. Although the leakage matrix changes throughout the year due to the B_0 angle variation, we assumed that over one year this variation averages out.

In Paper II, we developed and described a powerful test to check the correctness of the calculated leakage elements by looking directly in the observed Fourier spectra, namely the *cross echelle diagram*. It was applied to the GONG data with success, in particular for $l = 1$ and 2 modes.

2.3. Noise covariance matrix estimation

The noise covariance matrix B (Eq. 2) could be determined by an expression similar to the leakage matrix (see Schou & Brown 1994 and Paper I). In fact its elements, for which $l + l' + m + m'$ is odd, are zero in the same way as for the leakage matrix elements (Papers I and II). Another way to calculate the noise covariance matrix, and one which will be used here, is to estimate it directly from the cross spectrum outside the p-mode band. Unfortunately, the different source of solar and instrumental noise introduces a frequency dependence in the noise covariance elements. It is thus not obvious which part of the frequency spectrum to use. As the p modes are equally spaced in frequency, the noise covariance is calculated in between the modes with radial order n and $n + 1$ to avoid a possible spurious frequency dependence. This is a tricky task because we have to be aware of the spurious modes present in the Fourier spectrum of the target mode, particularly, of modes with a different degree. However, the spherical harmonic decomposition is very efficient for modes with a degree very different from the target mode.

To calculate the noise covariance between the $2l + 1$ Fourier spectra within a multiplet with a given (n, l) , we selected windows of approximately $20 \mu\text{Hz}$ width in between its central frequency $\nu_{n,l}$ and the adjacent ones $\nu_{n+1,l}$ and $\nu_{n-1,l}$, carefully avoiding frequency regions where there are modes with a degree l' where $|l' - l| \leq 5$. We used windows as large as possible to average out higher l modes which could be present in the spectra with a very small amplitude. In practice, these windows are better visualized in an echelle diagram centered on the target degree and containing all modes with l' not very different from the target l .

Instead of estimating the noise covariance directly, we computed the ratio of the noise covariance matrix \mathcal{R} because it varies

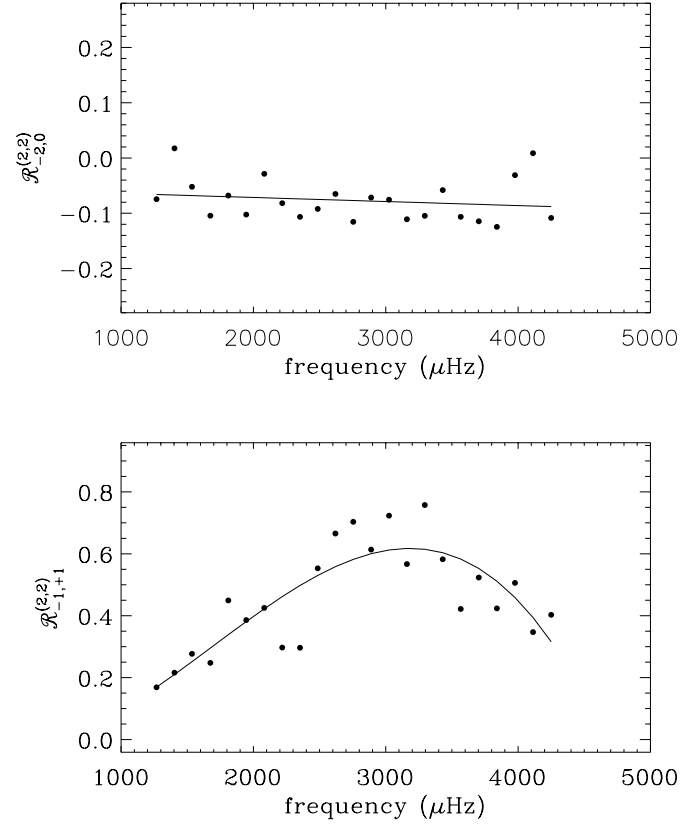


Fig. 2. Measured averages of the ratio cross spectrum (circles) for $l = 2$. On the *top*, $m = -2$ and $m' = 0$. On the *bottom*, $m = -1$ and $m' = +1$. Their frequency dependence is clearly seen. The continuous line is the polynomial fitting.

slowly with frequency and we can, in most cases, fit a straight line to its frequency dependence:

$$\mathcal{R}_{m,m'}^{(l,l')}(\nu) \equiv \frac{B_{m,m'}^{(l,l')}(\nu)}{B_{m,m}^{(l,l)}(\nu)} \approx \left\langle \frac{\text{Re} [y_{l,m}(\nu) y_{l',m'}^*(\nu)]}{y_{l,m}(\nu) y_{l,m}^*(\nu)} \right\rangle \quad (5)$$

where the average is over the $20 \mu\text{Hz}$ windows defined above and selected for each radial order n . The average inside the selected window of the ratio cross spectrum within a multiplet with a given (n, l) is calculated and plotted against frequency (see Fig. 2 for an example). The frequency dependence introduced by different sources of solar and instrumental noise is larger in some of the noise covariance matrix elements than others. We find that a polynomial of degree 1 and, in some cases, of degree 3 are a good fitting to $\mathcal{R}_{m,m'}^{(l,l)}(\nu)$. The theoretical calculation of the noise covariance matrix taking into account the solar and instrumental noise would be desirable to fully understand the $\mathcal{R}_{m,m'}^{(l,l)}(\nu)$ behaviour; however, this is outside the scope of this paper.

Note that $B_{m,m}^{(l,l)}(\nu)$ is the noise level of the observed power spectrum: $N_{l,m}(\nu)$. Thus, the noise covariance matrix is constructed using the estimated ratio cross spectrum:

$$B_{m,m'}^{(l,l)}(\nu) = N_{l,m}(\nu) \mathcal{R}_{m,m'}^{(l,l)}(\nu). \quad (6)$$

3. Source of systematic errors

3.1. Fourier versus power spectra fitting

In Paper I, using Monte-Carlo simulation, we showed that there is no bias on the p-mode frequency determination using the power or Fourier fitting, while the splitting coefficients derived fitting the power spectra for $l = 1$ are slightly overestimated with a bias of about 10 nHz. Besides, the uncertainties of the fitted splitting coefficients for $l \leq 2$ modes are larger when fitting the power spectra and similar for $l = 3$ (see Fig. 8 in Paper I). These predict quite well the differences between the two techniques when applied to the observations presented here.

For $l = 1$, the splitting coefficients found fitting the power spectra present a larger range of values and their weighted average over n is 16 nHz higher than the Fourier fitting (see Fig. 3). As expected, the differences between the two approaches diminish for higher degree modes. In fact, for $l = 2$, the weighted average over n of the a_1 splitting coefficient is higher by only 3 nHz fitting the power spectra and for $l = 3$, they agree quite well.

We can conclude that the Fourier fitting is very important in determining $l = 1$ mode parameters and still important for $l = 2$ modes because it calculates all their parameters with the smallest bias and error bars. On the other hand, and despite the fact that no improvement was found for $l = 3$ modes fitting the Fourier spectra, which will probably be true for higher degree modes, it is still advisable to fit the Fourier spectra instead of the power spectra. Fitting Fourier spectra will considerably reduce the bias on the splitting coefficients.

3.2. Influence of the leakage matrix on the splitting coefficients determination

The correct calculation of the leakage matrix is particularly important in the determination of the splitting coefficients. A change in the values assumed for the leakage matrix elements will introduce systematic effects on the estimated splitting coefficients fitting the Fourier or the power spectra. This could be one of the reasons for the discrepancies between the measurements of the splitting coefficients by different instruments with spatial resolution. However, the central frequencies will not be affected by these changes (see also Paper I).

In Paper I, we estimated mode parameters for $l = 1$ and 2 by fitting the Fourier spectra of synthetic data using Monte Carlo simulation. We used values of the leakage matrix elements different from the known true ones and the systematic error made on the fitted splitting coefficients proved to be quadratic, which is a very interesting result.

Due to symmetry properties, for $l = 1$, there will be only one matrix element to be determined, i.e. the leakage between $m = -1$ and $m = +1$, which we called α . We undertook the same exercise here, using values of α different from that of the theoretical value α_{th} (Sect. 2.2), the a_1 splitting coefficient was determined by fitting both the Fourier spectra and the power spectra (Fig. 4), obtaining results for the Fourier fitting with the same order of variation as found in the simulations. While the

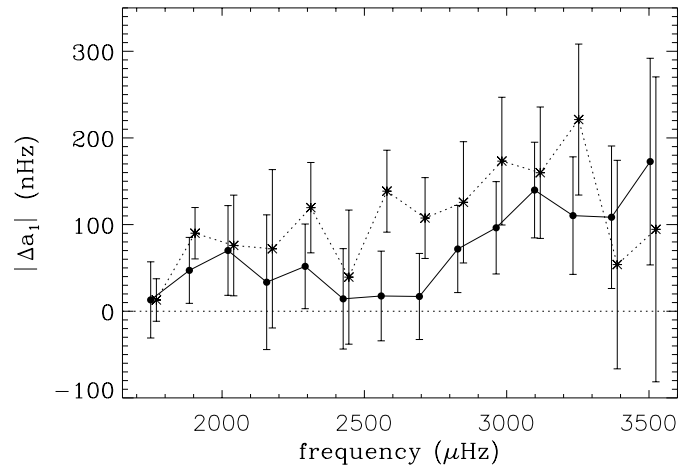


Fig. 3. Absolute difference between the a_1 coefficients and its weighted mean over n for $l = 1$ fitting the power spectra (stars) and the Fourier spectra (full circles). They are slightly displaced in frequency for a better visualization. The weighted average values fitting the power and the Fourier spectra are, respectively, 466 ± 27 nHz and 450 ± 19 nHz (in sidereal units).

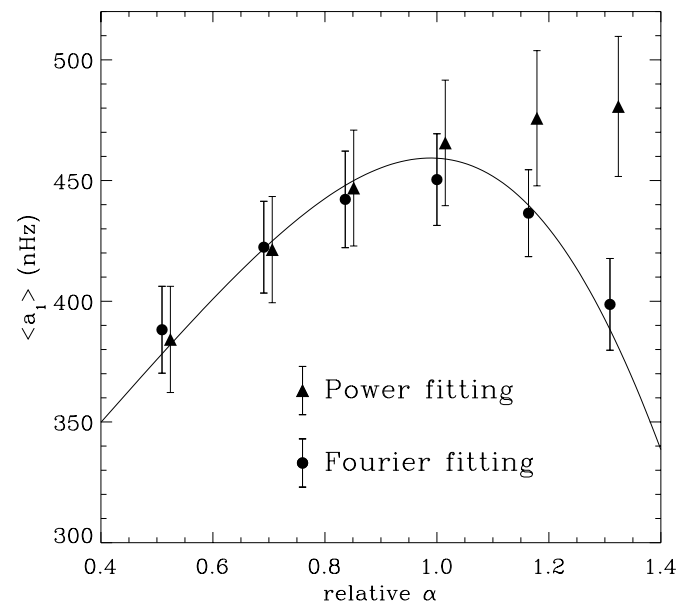


Fig. 4. Weighted average over n of sidereal a_1 for $l = 1$ as a function of the relative leakage α ($\alpha/\alpha_{\text{th}}$), where $\alpha_{\text{th}} = -0.55$. The full circles are found fitting the Fourier spectra and the triangles fitting the power spectra. The continuous line is the non-linear squares fit of the theoretical calculation (Eq. 7) to the a_1 weighted average (full circles).

a_1 coefficients calculated using the power spectra vary almost linearly with α , those found using the Fourier spectra obey a quadratic law. Thus, when fitting the Fourier spectra, the a_1 coefficient could only be underestimated using an incorrect value for α ; its correct value corresponds to the maximum value of the a_1 coefficient. Although these variations in the splitting coefficient are small in comparison to their error bars (around 15 nHz for an error of 20% in α), they are significant because of their systematic nature.

We have analytically derived the dependence of a_1 upon α fitting the Fourier spectra for $l = 1$. This was done by calculating the derivative of the logarithm of the likelihood function (S) with respect to a_1 , and equating this derivative to zero. The variation of the amplitudes, linewidth, central frequency and background noise using different values for α proved to be very small in the fitting and were neglected. The expression of a_1 as a function of α is given by (see Appendix A):

$$a_1 = a_1^c \frac{(\alpha\alpha^c - 1)^2 - (\alpha - \alpha^c)^2}{(\alpha\alpha^c - 1)^2 + (\alpha - \alpha^c)^2} \quad (7)$$

where α^c and a_1^c are the nominal values of α and a_1 respectively. Note that when $\alpha = \alpha^c$, a_1 will be equal to a_1^c and a_1^c is the maximum of the function. The continuous line in Fig. 4 is the non-linear squares fit of the theoretical calculation (Eq. 7) to the a_1 weighted average (full circles), which gives: $a_1^c = 459 \pm 8$ nHz and $\alpha^c = -0.54 \pm 0.02$. Note that the estimated uncertainties in the fitted a_1 coefficients for each α are correlated; however, as they are very similar, we used the same weight for all points in the fitting and the estimated a_1^c and α^c and their errors are an approximation. These values agree quite well with the Fourier fitting using the theoretical leakage matrix element $\alpha_{\text{th}} = -0.55$: $a_1 = 450 \pm 19$ nHz.

As a conclusion, we can say that the quadratic dependence of the rotational splittings upon the leakage elements is another reason to fit the Fourier spectra instead of the power spectra. Although Eq. (7) is only an approximation, it could be used to calculate the splitting coefficient or at least its weighted average with more precision, independently of the correctness of the leakage within a multiplet. However, in the next section we are going to show that in our case $a_1^c = 459 \pm 8$ nHz is still biased because of modes aliasing with different degrees. We limited ourselves in this section to the analysis of $l = 1$ where the leakage between the modes is more critical.

3.3. Leakage between modes of different degrees

So far we have mentioned only the leakage between the elements of a given multiplet. However, it is also possible to have leakage between modes of different degrees, i.e. aliasing modes. The leakage will be due to modes with a degree similar to the target mode; modes with a very different degree will have a negligible amplitude in the target spectrum. On the other hand, we will be concerned by the leakage of modes that have a frequency close to that of the target mode in the range ~ 1500 to 4000 μHz . To identify the aliasing modes, we plotted the mode frequencies in an echelle diagram (Fig. 5). We can see that the $l = 6$ modes overlap in frequency with the $l = 1$ and $l = 9$ modes, $l = 7$ modes overlap with $l = 4$ modes and so on.

The influence of the leakage of $l = 6$ and 9 modes in the determination of the $l = 1$ splitting coefficients can be clearly seen in Fig. 3 as a step for modes with $\nu > 2900$ μHz . However, as the mode degree increases, the fitting of the spectra becomes less sensitive to the leakage. In fact, for $l \geq 4$, it appears in the GONG data mainly as a second order effect: a bump in a_2 coefficients (Fig. 6a). These higher degree modes have many more

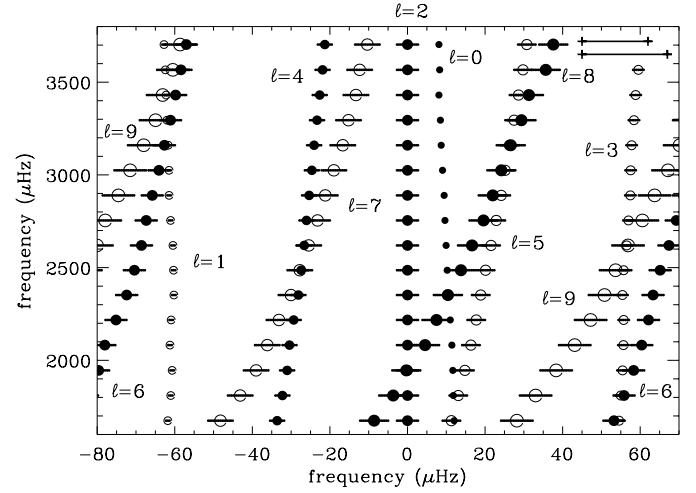


Fig. 5. Echelle diagram centered on $l = 2$. The even degree modes are indicated as full circles and the odd modes as empty circles. The size of the circles is proportional to its degree. The horizontal bar crossing each circle represents the splitting due to the solar rotation and has its approximate magnitude: $(2l + 1) \times 0.45$ μHz . The horizontal bars on the top right are the intervals where the modes are fitted: 17 μHz for $l \leq 2$ and 22 μHz for $l \geq 3$. The frequencies used here for $l \leq 6$ are the results of this paper (Sect. 4) and for $l > 6$ were obtained by the GONG project (Hill et al. 1996).

elements in the multiplet which enable a much better determination of their central frequencies and splitting coefficients, independently of the influence of the leakage, which is not, in the same way, present in the $(2l + 1)$ observed spectra of the multiplet. Modes with a degree which is different from the target by more than 3 have small amplitudes and seem not to affect the fitting, except for $l = 1$. The leakage of $l = 6$ into $l = 3$ and vice-versa, does not seem to affect the fitted parameters either. In addition, the leakage between $l = 0$ and $l = 2$ modes happens only at very high frequencies ($\nu > 3700$ μHz) and is not taken into account.

A straightforward way to consider the l leakage is to use a more complete leakage matrix in the likelihood function. Unfortunately, this is an extremely computer intensive task, because we have to fit multiplets with different degrees at the same time. We have instead constructed a more complete leakage matrix and applied its inverse to the observed Fourier spectra as described in Paper I and II: $\tilde{x} = C^{-1}y$ (Eq. 1), therefore obtaining the ‘cleaned’ spectra. This cleaning method produces spectra that are very nearly independent of each other, at least in making the leakage matrix close to the identity matrix. In this case, the two methods (power and Fourier fitting) will be identical (Paper I).

We constructed the leakage matrix for $l = 1, 6$ and 9 and used it to obtain their ‘cleaned’ spectra. Fig. 7 presents the splitting coefficients found fitting these ‘cleaned’ Fourier spectra (triangles), calculated in the same way as before (Fig. 3), except that here the leakage matrix is the identity matrix. The step mentioned earlier clearly disappeared.

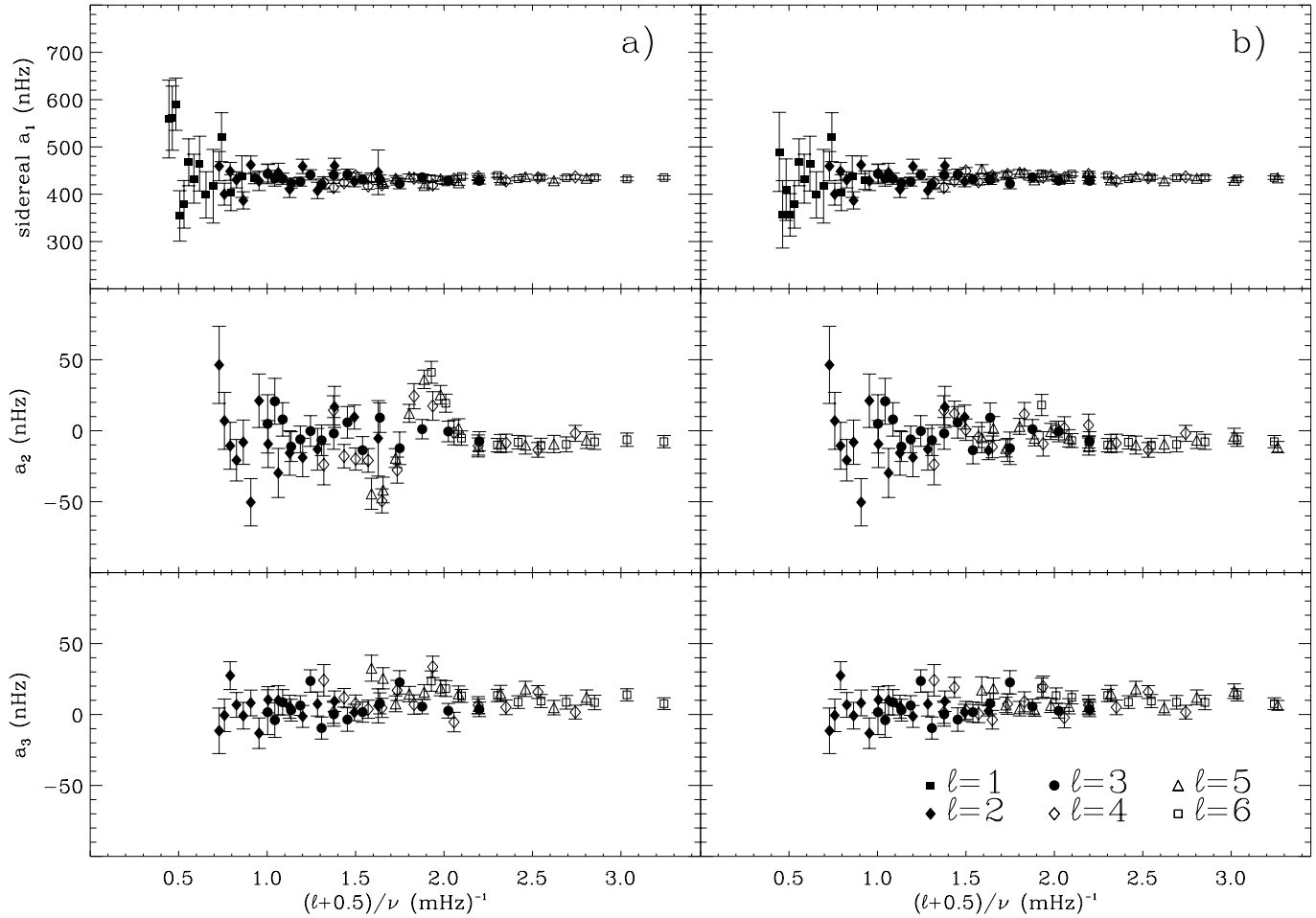


Fig. 6. **a** Splitting coefficients for the GONG data. Only modes with $\nu < 3500 \mu\text{Hz}$ were plotted. Note the step in the a_1 coefficients for $l = 1$ at $\sim 0.5 \text{ mHz}^{-1}$ and the bump in a_2 coefficient for $l \geq 4$ modes at $\sim 1.9 \text{ mHz}^{-1}$. **b** Same as **a**, except that the splitting coefficients of modes inside the leakage frequency range were found using spectra cleaned from aliasing degrees. Both features in a_1 and a_2 disappeared.

On the other hand, for $l \geq 4$ modes, the bump that appears in a_2 (Fig. 6a) at a given lower turning point could be caused by a solar physical process that is insensitive to the direction of propagation of the oscillations, such as an anisotropic sound speed or magnetic field at this solar radius, which will make the even coefficients be nonzero in their presence (Hill et al. 1991). Unfortunately, this curious feature is due to the leakage of $l = 7$ into 4, 8 into 5, and 9 into 6, i.e. between modes with $\Delta l = 3$ and $\Delta n = 1$. Although the leakage onto $l = 4, 5$ and 6 happens at different frequencies: 2456, 2914 and 3317 μHz respectively, they happen coincidentally at the same lower turning point: $r_t = c(r_t)/(2\pi)(l + 0.5)/\nu \approx 0.2R_\odot$. Applying the inverse of the complete leakage matrix to each pair, as in $l = 1$, and fitting the ‘cleaned’ spectra, the new splittings found no longer present the bump (Fig. 6b), proving that the bump is due to the leakage between the modes. Although there is still some structure around $(l + 0.5)/\nu \sim 1.9 \text{ mHz}^{-1}$, it could be due to an imperfect knowledge of the theoretical leakage matrix.

Comparing the fitted parameters using ‘cleaned’ and ‘uncleaned’ spectra, we found that the a_4 and a_5 splitting coefficients are the same (their determinations are very poor for such

low degree modes); a_1 , a_2 and a_3 splitting coefficients found fitting the ‘cleaned’ spectra are better than the ‘uncleaned’ ones inside the frequency interval of leakage in the sense that their values do not oscillate or else oscillate with smaller amplitudes (see Fig. 6b). The unperturbed frequencies are different mainly inside the leakage interval where their difference is less than $\sim 0.15 \mu\text{Hz}$ (Fig. 8).

As was already shown, it is very important to take the leakage of modes of different degrees into account. Using the inverse of the leakage matrix for cleaning the data is a simple way to solve this problem. However, outside the leakage frequency range of a given mode it is better to use the originally observed spectra (‘uncleaned’) as it is less manipulated and there is no necessity to use the ‘cleaned’ one. In Fig. 6b we plotted the parameters fitting the ‘uncleaned’ spectra, except for modes with (cf. Fig. 6): $l = 1$ and $\nu \geq 2963 \mu\text{Hz}$; $l = 4$ and $2051 \leq \nu \leq 3136 \mu\text{Hz}$; $l = 5$ and $\nu > 2641 \mu\text{Hz}$; and $l = 6$ and $\nu \geq 2961 \mu\text{Hz}$ where we used the ‘cleaned’ spectra. Besides, the ‘cleaned’ spectra have a higher background noise level than the ‘uncleaned’, whereas the mode amplitudes remain basically the same. This is going to affect essentially

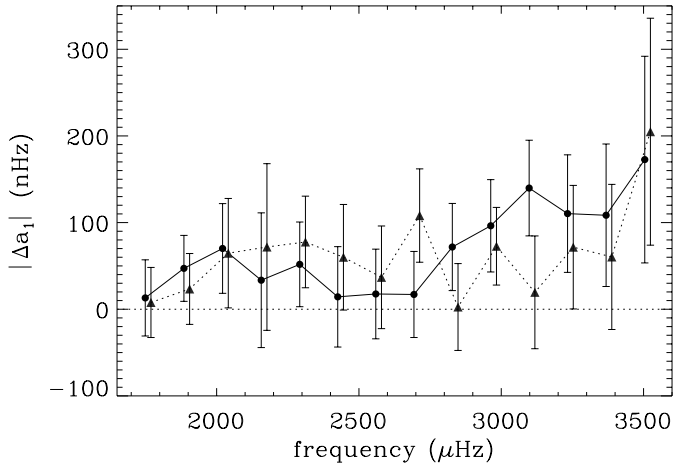


Fig. 7. Absolute difference between the a_1 coefficients and its weighted mean over n for $l = 1$ fitting the observed Fourier spectra (circles) and the ‘cleaned’ Fourier spectra (triangles). They are slightly displaced in frequency for a better visualization. The weighted average values fitting the observed and the ‘cleaned’ Fourier spectra are, respectively: 450 ± 19 nHz and 429 ± 17 nHz (in sidereal units). The full circles are the same as in Fig. 3.

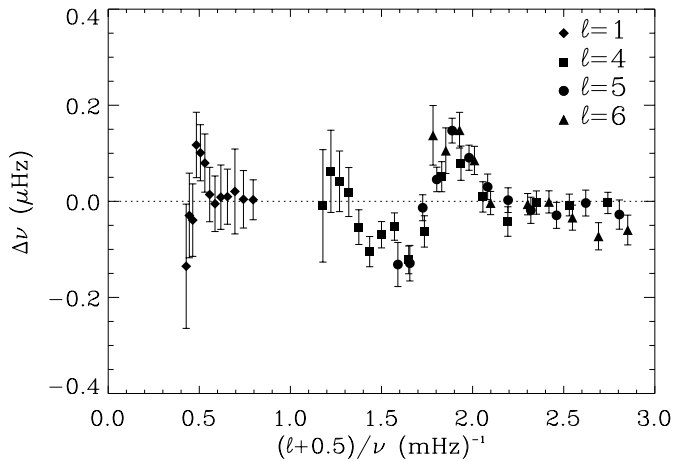


Fig. 8. Differences of frequencies between those found fitting the ‘cleaned’ spectra and those fitting the ‘uncleaned’ spectra ($\nu_{\text{cleaned}} - \nu_{\text{uncleaned}}$).

the determination of $l = 5$ and 6 modes with high frequency ($\nu > 3600$ μHz) where the signal-to-noise ratio is poor anyway.

4. Results

We will now describe our final results of the fitting of the low degree ($l \leq 6$) p-mode parameters using the GONG data and demonstrate that their determination is better than others found in the literature. In summary, we fitted the Fourier spectra instead of the power spectra for all l , except for $l = 0$. The leakage and the noise covariance matrices were calculated as described in Sects. 2.2 and 2.3, respectively. The variance of the spectrum of a single mode, v_{lm} , was represented by a Lorentzian profile (Eq. 3). In our preliminary results (Rabello-Soares & Appourchaux 1998), we used the ‘cleaned’ spectra for all modes with

$l = 1, 4, 5$ and 6 . However, here we are going to use the ‘cleaned’ spectra only for modes inside the leakage frequency range, as discussed in Sect. 3.3.

By estimating accurately the low degree p-mode parameters using high spatial resolution data, we enabled the creation in the future of a homogeneous set of frequencies and rotational splittings for estimating the solar structure and rotation profile.

4.1. Frequencies

The frequency results are shown in Table 1. We have identified 139 p modes with $l \leq 6$ (81 with $l \leq 3$) with an estimate of the uncertainties on the fitted frequency of less than 0.2 μHz . Frequencies in parenthesis were positively identified using the collapsogramme technique described by Appourchaux (1998) but could not be fitted properly due to their narrow linewidths; the error bars are rough estimates taking into account the frequency resolution and the $2l + 1$ number of modes.

We have compared our frequencies with those of the GONG project for a three-month time series starting on 6 June 1996, which is essentially contained within the period used here. In that analysis, the power spectra was fitted instead of the Fourier spectra and the leakage between the elements of a multiplet was not taken into account (Hill et al. 1996). Its number of identified modes for $l \leq 3$ is very small. Out of the 55 frequency determinations in common with ours for $l \leq 6$, 93% coincide within 3σ (using combined errors), 82% within 2σ and 55% within 1σ .

We have compared our frequencies with those of the GOLF instrument on board the SOHO satellite (Lazrek et al. 1997) which performs full-disk integrated light velocity measurements. They used an eight-month observational period, of which four overlap with the GONG observations used here. Their frequencies are in good agreement with ours. Out of the 72 frequency determinations in common with ours for $l \leq 3$, 100% coincide within 3σ (using combined errors), 93% within 2σ and 71% within 1σ , meaning that the scatter is due to a normally distributed noise. For $l = 0$, the estimate of the uncertainties on the fitted GOLF frequency is similar to ours for the same modes but for $l = 1, 2$ and 3 , they are significantly larger than ours, approximately 2^l times larger. This is due to a combination of different signal-to-noise ratios, modes detected and length of observing time. In addition, the GOLF frequency errors are the average of statistical errors in the fittings done for different authors. Last but not least, the time series for $l = 0$ in the GONG data analysis is calculated in a different way than the other degrees; it is obtained through the spatial average of each solar image, in such a way that, for $l = 0$, GONG simulates an integrated light instrument. In the $l = 0$ fitting, the $l = 2$ modes were fitted simultaneously. This is necessary not only for modes with $\nu \geq 3600$ μHz where the $l = 2$ modes overlap the $l = 0$ modes but also for modes with $\nu \geq 2800$ μHz . Otherwise, the background noise level will be overestimated due to the $l = 2$ modes, causing a decrease in $l = 0$ linewidths. The $l = 2$ fitted parameters are consistent with those found using spherical

Table 1. Frequencies and errors in μHz as measured by GONG. Frequencies in parenthesis were positively identified but could not be fitted properly.

n	$\ell=0$	$\ell=1$	$\ell=2$	$\ell=3$	$\ell=4$	$\ell=5$	$\ell=6$
6						(1254.52±0.02)	(1295.49±0.02)
7				(1306.75±0.02)	(1356.37±0.02)	(1401.65±0.02)	1443.76±0.01
8			(1394.67±0.03)	(1451.00±0.02)	(1500.29±0.02)	1545.28±0.01	1587.47±0.01
9		(1472.83±0.04)	1535.85±0.01	1591.54±0.01	1640.92±0.02	1685.84±0.01	1727.76±0.01
10		1612.74±0.02	1674.53±0.01	1729.08±0.01	1778.02±0.01	1823.36±0.02	1866.10±0.01
11	1686.55±0.01	1749.24±0.04	1810.26±0.02	1865.27±0.01	1914.70±0.02	1960.54±0.02	2004.04±0.02
12	1822.08±0.06	1885.06±0.03	1945.73±0.03	2001.18±0.02	2051.65±0.02	2098.43±0.02	2142.46±0.02
13	1957.42±0.07	2020.84±0.04	2082.07±0.02	2137.74±0.02	2188.28±0.02	2235.35±0.02	2279.76±0.02
14	2093.52±0.08	2156.69±0.06	2217.62±0.02	2273.36±0.02	2324.03±0.02	2371.05±0.02	2415.47±0.02
15	2228.65±0.06	2291.94±0.04	2352.16±0.03	2407.58±0.02	2458.46±0.02	2506.02±0.02	2551.02±0.02
16	2362.79±0.06	2425.57±0.05	2485.88±0.03	2541.61±0.02	2592.97±0.02	2641.14±0.02	2687.02±0.02
17	2496.12±0.06	2559.14±0.04	2619.60±0.03	2676.13±0.02	2728.34±0.02	2777.27±0.02	2823.69±0.02
18	2629.56±0.06	2693.31±0.04	2754.38±0.03	2811.37±0.02	2864.13±0.02	2913.65±0.02	2960.61±0.01
19	2764.05±0.06	2828.02±0.05	2889.48±0.03	2946.95±0.02	3000.04±0.02	3049.86±0.02	3097.19±0.02
20	2898.94±0.05	2963.22±0.04	3024.69±0.02	3082.22±0.02	3135.78±0.02	3186.15±0.02	3233.88±0.02
21	3033.72±0.05	3098.15±0.05	3159.85±0.03	3217.65±0.03	3271.66±0.03	3322.47±0.03	3370.84±0.03
22	3168.54±0.06	3232.98±0.05	3294.98±0.03	3353.38±0.03	3407.99±0.04	3459.25±0.03	3508.08±0.03
23	3303.47±0.07	3368.40±0.06	3430.62±0.05	3489.45±0.04	3544.59±0.04	3596.26±0.05	3645.91±0.04
24	3438.72±0.10	3504.07±0.10	3566.48±0.07	3626.01±0.06	3681.61±0.06	3733.69±0.06	3783.76±0.06
25	3574.77±0.15	3640.15±0.13	3702.93±0.09	3762.80±0.08	3818.73±0.08	3871.61±0.08	3921.86±0.08
26	3711.03±0.49	3775.66±0.18		3899.75±0.11	3956.31±0.12	4009.77±0.12	4060.56±0.11
27	3846.92±0.36			4036.78±0.16	4093.82±0.19		
28	3984.45±0.45			4173.92±0.10			

harmonic decomposition; however, they were not used in this work.

We also compared our results with the LOWL data, which is a one-site instrument. The data we used was velocity measurements (125 square pixels), starting in February 1995 and it is one-year long, thus having a six-month overlap with the GONG data used here (Tomczyk et al. 1995). Out of the 87 LOWL frequency determinations for $l \leq 6$, 93% coincide within 3σ (using combined errors), 72% within 2σ and 45% within 1σ .

Despite the good agreement between the frequency determination, the GONG frequencies are systematically lower than GOLF and LOWL frequencies. The weighted average of the frequency differences between our work and LOWL is $0.037 \pm 0.005 \mu\text{Hz}$ (87 observations) and between our work and GOLF $0.03 \pm 0.01 \mu\text{Hz}$ (72 observations). The LOWL observational period is slightly further away from the solar minimum, which occurred at the beginning of 1996, than the GONG observations used here. Its frequency difference is in agreement with a decrease in frequency of $\sim 0.4 \mu\text{Hz}$ between solar maximum and minimum found by several authors (Hill et al. 1991). Even though the GOLF observational period is inside the solar minimum, its frequency difference is barely significant.

4.2. Splitting coefficients

Fig. 6b shows the splitting coefficients results found for $l = 1$ up to 6 as a function of the lower turning point position. The coefficients for $l = 1$ and high-order $l = 2$ modes are very scattered and have larger error bars than the others. The small

number of elements in the multiplets and the very small value of the splitting, of the order of 10 times the uncertainty in the mode frequency, impose difficulties on the splitting determination. This scattering in the splitting coefficients determination is also present in the analysis of a very low spatial resolution instrument, LOI/SOHO (Appourchaux et al. 1998c), and in integrated light instruments.

The splitting for the three-month GONG series is poorly determined. This is probably due to the short period of observation and the incorrect treatment of the mode leakage. However, it agrees with our results towards higher degree modes. The weighted averages over n of sidereal a_1 coefficients are: $257 \pm 18 \text{ nHz}$ for $l = 1$ (3 observations), $328 \pm 27 \text{ nHz}$ for $l = 2$ (4 observations), $397 \pm 18 \text{ nHz}$ for $l = 3$ (6 observations), $427 \pm 11 \text{ nHz}$ for $l = 4$ (9 observations), $430 \pm 6 \text{ nHz}$ for $l = 5$ (7 observations) and $438 \pm 7 \text{ nHz}$ for $l = 6$ (7 observations), which could be compared with the results found here (see Table 2).

When compared with GOLF determinations (Lazrek et al. 1997), our error bars are smaller and our measurements are similarly scattered for $l = 1$ modes. However, for $l = 2$ and 3 modes, our data are less scattered and the error bars are much smaller.

4.3. Linewidths

Finally, the estimated linewidth γ_{nl} (Eq. 3) of the modes obtained from the fit are shown on Fig. 9. The power-law behaviour of the linewidths is clearly visible for all degrees at the low

Table 2. Weighted averages over sidereal a_1 splitting coefficient values of the modes with the same l and their errors (in nHz).

	$l = 1$	$l = 2$	$l = 3$
n	10–26	9–25	9–28
	425.2 ± 9.8	432.6 ± 4.8	431.2 ± 2.0
	$l = 4$	$l = 5$	$l = 6$
n	9–27	8–26	7–26
	434.9 ± 1.9	435.1 ± 1.4	435.2 ± 1.1

and high frequency limits: $\gamma \propto \nu^{5.24 \pm 0.01}$ (28 observations) for $\nu \leq 2122 \mu\text{Hz}$ and $\gamma \propto \nu^{9.042 \pm 0.003}$ (41 observations) for $\nu \geq 3134 \mu\text{Hz}$ from an error-weighted fit to the data. At intermediate frequencies, there is a small depression in the linewidth around $2900 \mu\text{Hz}$ which is predicted by theory (Balmforth 1992) and first detected by Fröhlich et al. (1997).

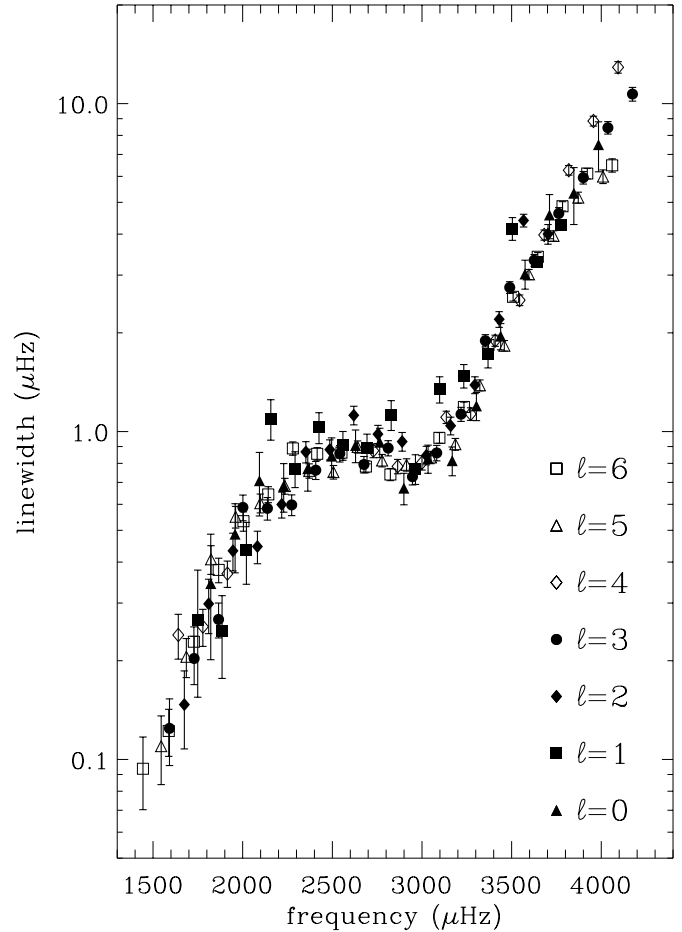
5. Conclusion

A more realistic approach was used to fit the helioseismic data, assuming that the observed spectra was statistically dependent upon one another (Fourier fitting). This is in contrast to what is done in general (power fitting), resulting in a more complete treatment of the leakage between the modes.

We studied different sources of systematic errors in the determination of the mode frequencies and rotational splittings. We showed that the Fourier spectra fitting will provide, especially for low-degree modes, splitting estimates that are far less biased than those derived by power spectra fitting. Moreover, we studied the effect upon the splitting determination of an imperfect knowledge of the leakage elements for $l = 1$, where the leakage determination is the most critical. While a_1 coefficients for $l = 1$ estimated using the power spectra vary almost linearly with the leakage, those found using the Fourier spectra obey a quadratic law. For very low degree modes, this quadratic dependence is another reason to fit the Fourier spectra instead of the power spectra. In addition, the effect of the leakage between modes of different degrees upon the p-mode frequencies and splitting coefficients determination was analyzed. A procedure for ‘cleaning’ the spatial alias is described which leads to frequencies and splitting coefficients with systematic errors smaller than before.

The results obtained here show significant improvement on previous GONG determinations especially for increasing the number of identified modes with $l \leq 6$ and for minimizing the bias on the splitting determination and the error bars. A timely implementation of the Fourier spectra fitting technique in the determination of the p-mode parameters provided by the GONG project would surely produce a scientific boost for the whole helioseismic community.

Acknowledgements. This work utilizes data obtained by the Global Oscillation Network Group (GONG) project, managed by the National Solar Observatory, a Division of the National Optical Astronomy Observatories, which is operated by AURA, Inc. under a cooperative

**Fig. 9.** Linewidths of the p modes.

agreement with the National Science Foundation. The data were acquired by instruments operated by the Big Bear Solar Observatory, High Altitude Observatory, Learmonth Solar Observatory, Udaipur Solar Observatory, Instituto de Astrofísica de Canarias, and Cerro Tololo Interamerican Observatory. We are thankful to S. Tomczyk and J. Schou for sending us the LOWL results of their analysis. We are also thankful to Anette Skovgaard and Kyla Hanington for proofreading the English. The work was supported in part by the Danish National Research Foundation through its establishment of the Theoretical Astrophysics Center.

Appendix A: calculation of the a_1 coefficient as a function of the leakage matrix for $l = 1$ fitting the Fourier spectra

According to Eq. (1), the observed Fourier spectra for $l = 1$, taking into account only the leakage within the multiplet, is given by:

$$\begin{pmatrix} y_{-1} \\ y_0 \\ y_{+1} \end{pmatrix} = \begin{pmatrix} 1 & 0 & \alpha^c \\ 0 & 1 & 0 \\ \alpha^c & 0 & 1 \end{pmatrix} \begin{pmatrix} x_{-1} \\ x_0 \\ x_{+1} \end{pmatrix} \quad (\text{A1})$$

where α^c is the leakage between $m = +1$ and $m = -1$ present in the observed spectra. The index that indicate the mode degree

and the order n are omitted. By analogy, the assumed leakage matrix for $l = 1$ will be:

$$C = \begin{pmatrix} 1 & 0 & \alpha \\ 0 & 1 & 0 \\ \alpha & 0 & 1 \end{pmatrix} \quad (\text{A2})$$

and, neglecting the noise covariance, the expected covariance matrix (Eq. 2) is equal to:

$$V = \begin{pmatrix} v_{-1} + \alpha^2 v_{+1} & 0 & \alpha(v_{-1} + v_{+1}) \\ 0 & v_0 & 0 \\ \alpha(v_{-1} + v_{+1}) & 0 & \alpha^2 v_{-1} + v_{+1} \end{pmatrix} \quad (\text{A3})$$

The variances v_m will be represented by a Lorentzian profile (Eq. 3):

$$\begin{aligned} v_{-1}(\nu_i) &= \frac{A_1(\gamma/2)^2}{(\gamma/2)^2 + (\nu_i + a_1)^2} \\ v_0(\nu_i) &= \frac{A_0(\gamma/2)^2}{(\gamma/2)^2 + \nu_i^2} \\ v_{+1}(\nu_i) &= \frac{A_1(\gamma/2)^2}{(\gamma/2)^2 + (\nu_i - a_1)^2} \end{aligned} \quad (\text{A4})$$

where $A_{|m|}$ is the power amplitude, γ is the full linewidth at half maximum, ν_i is frequency subtracting the ‘unperturbed’ mode frequency and a_1 is the rotational splitting coefficient as defined by Eq. (4). Assuming the probability density function of the observed Fourier spectra to be a multivariate normal distribution, the mode parameters will be found minimizing the logarithm of the likelihood of Eq. (32) in Paper I. Substituting the above equations for $l = 1$ into the logarithm of Eq. (32):

$$\begin{aligned} S &= \sum_i 2 \left(\frac{\alpha\alpha_c - 1}{\alpha^2 - 1} \right)^2 \left(\frac{x_{-1}^2}{v_{-1}} + \frac{x_{+1}^2}{v_{+1}} \right) \\ &+ \sum_i 2 \left(\frac{\alpha - \alpha_c}{\alpha^2 - 1} \right)^2 \left(\frac{x_{+1}^2}{v_{-1}} + \frac{x_{-1}^2}{v_{+1}} \right) \\ &+ \sum_i \ln [v_{-1}v_0v_{+1}(1 - \alpha^2)^2] \\ &+ \sum_i 2 \frac{x_0^2}{v_0} \end{aligned} \quad (\text{A5})$$

The sum will be over a frequency interval large enough to characterize the Lorentzians (Eq. A4) and centered at the central frequency of the multiplet. The process of finding the minimum of S means that any partial derivative of S with respect to any mode parameter must be 0. It is impossible to find an analytical solution that solves the set of equations involving the partial derivatives. Nevertheless, we have assumed that all other parameters are much less sensitive to the variation in α than the splitting a_1 . The variation of the amplitudes, linewidth and central frequency using different values for α are proved to be very small in the performed Fourier fittings (Sect. 3.2) and are neglected. The only functions of a_1 in Eq. (A5) are $v_{\pm 1}$ and:

$$\begin{aligned} \frac{\partial v_{-1}}{\partial a_1} &= -2 \frac{(\nu + a_1)}{A_1(\gamma/2)^2} v_{-1}^2; \\ \frac{\partial v_{+1}}{\partial a_1} &= 2 \frac{(\nu - a_1)}{A_1(\gamma/2)^2} v_{+1}^2 \end{aligned} \quad (\text{A6})$$

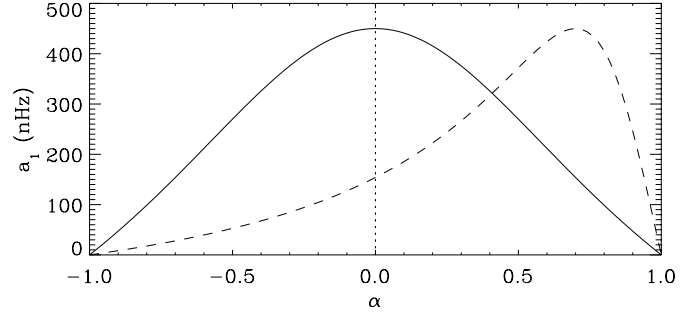


Fig. A1. Splitting coefficient a_1 as a function of α given by Eq. (A10) for $a_1^c = 450$ nHz. The continuous line is for $\alpha^c = 0$ and the dashed line is for $\alpha^c = 0.7$.

The partial derivative of S becomes:

$$\begin{aligned} \frac{\partial S}{\partial a_1} &= \frac{2}{A_1(\gamma/2)^2} \\ &\left\{ 2 \left(\frac{\alpha\alpha_c - 1}{\alpha^2 - 1} \right)^2 \sum_i \left[x_{-1}^2(\nu_i + a_1) - x_{+1}^2(\nu_i - a_1) \right] \right. \\ &+ 2 \left(\frac{\alpha - \alpha_c}{\alpha^2 - 1} \right)^2 \sum_i \left[x_{+1}^2(\nu_i + a_1) - x_{-1}^2(\nu_i - a_1) \right] \\ &\left. - \sum_i \left[v_{-1}(\nu_i + a_1) \right] + \sum_i \left[v_{+1}(\nu_i - a_1) \right] \right\} \end{aligned} \quad (\text{A7})$$

If the discrete summation over the frequency bins is replaced by an integral, the fitting is made at frequency intervals much larger than the true splitting (a_1^c) and the observed power spectrum (x_m^2) is replaced by its mean over several realizations (i.e. its Lorentzian profile which has the correct rotational splitting a_1^c), it is easy to show that:

$$\begin{aligned} \sum_i v_{-1}(\nu_i + a_1) &\simeq 0 \\ \sum_i v_{+1}(\nu_i - a_1) &\simeq 0 \\ \sum_i x_{-1}^2(\nu_i + a_1) &\simeq - \sum_i x_{+1}^2(\nu_i - a_1) \\ &\simeq -A_1 \frac{\gamma}{2} (a_1 - a_1^c) \pi \\ \sum_i x_{+1}^2(\nu_i + a_1) &\simeq - \sum_i x_{-1}^2(\nu_i - a_1) \\ &\simeq -A_1 \frac{\gamma}{2} (a_1 + a_1^c) \pi \end{aligned} \quad (\text{A8})$$

Substituting these equations into Eq. (A7) and making it equal to zero:

$$(a_1 - a_1^c) \frac{(1 - \alpha_c\alpha)^2}{(1 - \alpha^2)^2} + (a_1 + a_1^c) \frac{(\alpha_c - \alpha)^2}{(1 - \alpha^2)^2} = 0 \quad (\text{A9})$$

An expression of a_1 as a function of α is given by:

$$a_1 = a_1^c \frac{(\alpha\alpha^c - 1)^2 - (\alpha - \alpha^c)^2}{(\alpha\alpha^c - 1)^2 + (\alpha - \alpha^c)^2} \quad (\text{A10})$$

Note that when $\alpha = \alpha^c$, a_1 will be equal to a_1^c which is the maximum of the function. The function is symmetric around α^c

only when $\alpha^c = 0$ and could be approximated by a parabola. Otherwise, it is highly asymmetric (Fig. A1).

References

- Appourchaux T., 1998, In: Korzennik S.G., Wilson A. (eds.) ESA SP 418 - Structure and Dynamics of the Interior of the Sun and Sun-like Stars. ESA Publications Division, Noordwijk, The Netherlands, p. 37
- Appourchaux T., Gizon L., Rabello-Soares M.C., 1998a, A&AS 132, 107
- Appourchaux T., Rabello-Soares M.C., Gizon L., 1998b, A&AS 132, 121
- Appourchaux T., Toutain T., Telljohann U., et al., 1995, A&A 294, L13
- Appourchaux T. and the VIRGO team, 1998c, In: Korzennik S.G., Wilson A. (eds.) ESA SP 418 - Structure and Dynamics of the Interior of the Sun and Sun-like Stars. ESA Publications Division, Noordwijk, The Netherlands, p. 99
- Balmforth N.J., 1992, MNRAS 255, 603
- Duvall T.L., Harvey J.W., 1986, In: Gough D.O. (ed.) Seismology of the Sun and the Distant Stars. D. Reidel, Dordrecht, p. 105
- Fröhlich C., Andersen B.N., Appourchaux T., et al., 1997, Sol. Phys. 170, 1
- Harvey J.W., Hill F., Hubbard R.P., et al., 1996, Sci 272, 1284
- Hill F., Deubner F.-L., Isaak G., 1991, In: Cox A.N., Livingston W.C., Matthews M. (eds.) Solar Interior and Atmosphere. Space Science Series, University of Arizona Press, p. 329
- Hill F., Stark P.B., Stebbins R.T., et al., 1996, Sci 272, 1292
- Lazrek M., Baudin F., Bertello L., et al., 1997, Sol. Phys. 175.2, 227
- Pijpers F.P., 1997, A&A 326, 1235
- Rabello-Soares M.C., Appourchaux T., 1998, In: Korzennik S.G., Wilson A. (eds.) ESA SP 418 - Structure and Dynamics of the Interior of the Sun and Sun-like Stars. ESA Publications Division, Noordwijk, The Netherlands, p. 299
- Rabello-Soares M.C., Roca Cortés T., et al., 1997, ApJ 480, 840
- Schou J., 1992, On the Analysis of Helioseismic Data. Ph.D. Thesis, Aarhus University, Aarhus, Denmark
- Schou J., Brown T.M., 1994, A&AS 107, 541
- Tomczyk S., Schou J., Thompson M.J., 1995, ApJ 448, L57